Design, assembly and validation test of a sub-1Amp LaB6 hollow cathode

IEPC-2024-805

Presented at the 38th International Electric Propulsion Conference, Toulouse, France
June 23-28, 2024

Antonio Montero Barriga* and Tatiana Perrotin †
and Jaume Navarro Cavallé ‡
Universidad Carlos III de Madrid, Avenida de la Universidad 30, Leganés, Madrid, 28911, Spain

and
Xin Chen §
Universidad Rey Juan Carlos, Camino del Molino 5, Fuenlabrada, Madrid, 28942, Spain

This research inquires into the design, manufacturing, assembly, and validation test of a new sub-1 Amp LaB_6 hollow cathode intended to be coupled with low-power class Hall Thrusters (100 - 200 W), which are currently being developed at the Universidad Carlos III de Madrid. This manuscript summarises the main results of this experimental campaign providing, among other results, its characteristic heater current-voltage curve, power consumption, and heating power during the ignition protocol. The first experimental campaign of the cathode in diode mode has proven its capability for delivering electrical current in the range 0.8 - 2.5 Amp, fed with Xenon (0.8 - 1.5 sccm), self-heated, with floating keeper and discharge power about 130 W. The test has proven as well a cumulative operation of more than 10 hours with no degradation.

I. Introduction

In the last decades, there has been a constantly increasing development of space missions and investment in this sector, in which Electric Propulsion (EP) has played a vital role due to its higher specific impulse (I_{sp}) compared to Chemical Propulsion. Nowadays the rise of satellite telecommunications and mega-constellations at LEO, such as OneWeb or Starlink, has led to an exponential increase on the demand of space technologies. Even before the NewSpace age started, the miniaturisation needs had driven EP developers to scale down existing EP technologies. This has been the case of the Hall thruster, and its necessary neutraliser. In this context, low-current Hollow Cathodes (HC) have become a need as an electron source for ionization and plume neutralization, for thrusters ejecting a non-neutral particle beam such as Hall thrusters and gridded ion thrusters, among others. Therefore, the EP community has focused as well in developing low-current HCs as demonstrated by the work of Lev[1], Pedrini[2], Goebel[3], Domonkos[4] or Potrivitu[5]. Low-current Hollow Cathode configurations for 1 A discharge current feature both heaterless architectures and conventional designs with a heater. For the insert material, many researchers still use the standard thermionic materials, LaB_6, BaO-impregnated tungsten, or promising ones such as the electride C12A7:e- because of their low work function[6].

In this frame, the Universidad Carlos III de Madrid started to develop cylindrical hall thrusters (CHT) in the 200 W range[7;8]. This CHT requires the use of an appropriate cathode as neutralizer that is able to provide a sufficient amount of current ($\sim$ 1 A), while keeping a low propellant consumption (below 1 sccm

*Master Student and Performance Engineer at ITP Aero, Department of Aerospace Engineering, Universidad Carlos III de Madrid, tonimb11@gmail.com
†Phd Candidate, Department of Aerospace Engineering, Universidad Carlos III de Madrid, and tperroti@pa.uc3m.es
‡Associate Professor, Department of Aerospace Engineering, Universidad Carlos III de Madrid, and janavarr@ing.uc3m.es
§Assistant Professor, Department of Signal Theory and Communications, Universidad Rey Juan Carlos, and xin.chen@urjc.es

of Xenon). Since it is a cathode for experimental use only, there are no hard requirements regarding the HC power consumption. Nevertheless, the functional requirement of being able to operate in the self-sustained mode has been considered from the early design stages, i.e. the HC should operate without heater power and with a floating keeper after ignition.

The commercial availability of hollow cathodes with these specifications is scarce, this motivates the in-house development of a HC to cope with the CHT requirements. This manuscript will briefly present the full process of HC design, assembly, integration and validation test. The document is organised as follows, Section II summarises the trade-off and HC design, the final configuration is shown in Section III. The experimental setup is described in Section IV, and the main results are highlighted in Section V. Conclusions are wrapped up in the last section.

II. Hollow Cathode design process

A Hollow Cathode (HC) is composed of an insert or emitter material enclosed within a refractory metal cathode tube, with a winded heater filament and an external keeper electrode. The insert (4 in Fig. 1), which emits electrons through thermionic emission mechanism, typically uses a low work function material such as Lanthanum Hexaboride (LaB_6), Barium Oxide-impregnated Tungsten (BaO-W) or Calcium aluminate electride (C12A7:e-). The lower the work function of the material, the lower the temperature required for electron emission. Being the innermost layer, the insert is typically a hollow cylinder whose dimensions (internal diameter and length) define the emission area[5]. The cathode tube (2 in Fig. 1), a conductive material electrically connected to the insert, is the negative electrode that sets the potential reference for the keeper and the external anode bias. This potential reference can be electrically grounded or floating. Thermal shields (13 in Fig. 1) can usually be found outside the cathode tube layer to reduce thermal losses and sustain thermionic emission. The keeper (3 in Fig. 1), being the outermost layer is biased at a high positive potential with respect to the cathode, thus, it establishes a strong electric field, which facilitates the HC ignition by extracting electrons from the emitter. It also protects the internal cathode components from ion bombardment and other kinds of contamination[9;10].

For low-current applications, the design usually features a small cathode orifice with an orificed keeper separated by a small distance. According to Goebel et al.[3], the smaller the orifice, the greater the internal gas pressure. The resulting orifice heating leads to more ionization in the emitter region, increased plasma density, and thus more electron emission. Typically, the electron density is about 50 % higher at the downstream end of the orifice than at its upstream end. Additionally, a smaller keeper orifice reduces the required mass flow rate to sustain the discharge[10].

To achieve an insert temperature sufficiently high for thermionic emission, a heater (19 in Fig. 1) made of a resistive filament is typically used at ignition. The complex heater design not only needs good electrical insulation along the filament but also demands efficient heat transfer towards the insert. In addition, it must be able to withstand high temperatures, to avoid melting and short circuits. The reliability of the heater is crucial for ensuring successful operation and long lifetime of a conventional HC[11]. After a discharge is established, the steady-state operation can be self-sustained by the ion-bombardment heating inside the hollow cavity and the heater can be shut down. Nevertheless, the power consumption required for ignition still poses an important constraint on HC performance. An alternative to this conventional configuration is the Heaterless Hollow Cathodes (HHC) that achieves ignition only by applying a high potential difference between the keeper and cathode[9;12].

A. Trade-off and design choices

During the design process of this HC device, a trade-off analysis among several HC design architectures, components, and materials was performed to identify the optimal configuration for the requirements established.

1. Insert material

The three main candidates of insert materials (LaB_6, BaO-W, and C12A7:e-) have work function of 2.67 eV, 2.1 eV, and 2.4 eV, respectively[6;13;14]. The BaO-impregnated Tungsten has the lowest work function which allows it to achieve a current density of $10^5\,\mathrm{A\,m^{-2}}$ at a temperature around 1100 °C, therefore relaxing the thermal and power requirements[14;15]. Nevertheless, it is sensitive to poisoning and impurities, which

makes it challenging to handle and can result in an increase of the work function during operation and thus hampers the HC performance. The Calcium aluminate electride C12A7:e-, appears promising for future applications due to its enhanced robustness to impurities while maintaining similar emission efficiencies [6;16]. Lanthanum Hexaboride has the highest work function, it requires an emission temperature of around 1500 °C to achieve 10^5 A/m^2. Despite its higher temperature for emission, LaB_6, has been widely used in HC design and extensively tested. It exhibits superior resistance to poisoning, demonstrates suitability for "low" purity gases, and showcases robust performance and enduring longevity in existing HC devices [17;18;19].

As a trade-off, prioritising lifetime and robustness, the final material selected was LaB_6. This decision also considers that the insert material may be exposed to ambient conditions because the HC will be frequently disassembled for component replacement and design improvements during laboratory testing. To further enhance robustness, a graphite layer (5 in Fig. 1) is inserted between the insert and the cathode tube to inhibit Boron diffusion from LaB_6 to the cathode refractory metal, which would increase the work function. [13;18].

2. Hollow cathode main dimensions

For any orificed HC design the dimensions which most determine the operation of the device are the orifice diameter, the insert cylinder dimensions, the keeper-emitter distance, the keeper orifice diameter and the overall cathode length. These dimensions, for the HC presented in this work, are gathered in Table 1.

Fig. 1 shows the cross-sectional view of the developed HC design [20]. The labels from 1 to 20 in Fig. 1 identify each HC part listed in Table 2. Note that shoulder bushings and fasteners are not listed as parts.

Most of the selected materials are refractory metals and ceramics such as Alumina, Boron Nitride and Molybdenum. They have low thermal conductivity to sustain operating temperatures over 1400 K while maintaining a high thermal efficiency. The keeper base, cylinder and orifice plate are machined as a single graphite part to ensure good electrical conduction and sustain high temperatures. Also it has to withstand the electric arc during the ignition process of around 500 - 600 V.

An innovative aspect of the present HC design is its modularity and interchangeable design without any welded part. This allows to replace any damaged components and to modify performance dimensions such as the orifice and keeper orifice diameters, insert length, or keeper to orifice distance. For this purpose most of the components are either bolted to the base flange or held by compression forces between sleeves and disks. Alumina bushings are used to avoid short circuits between electric components.

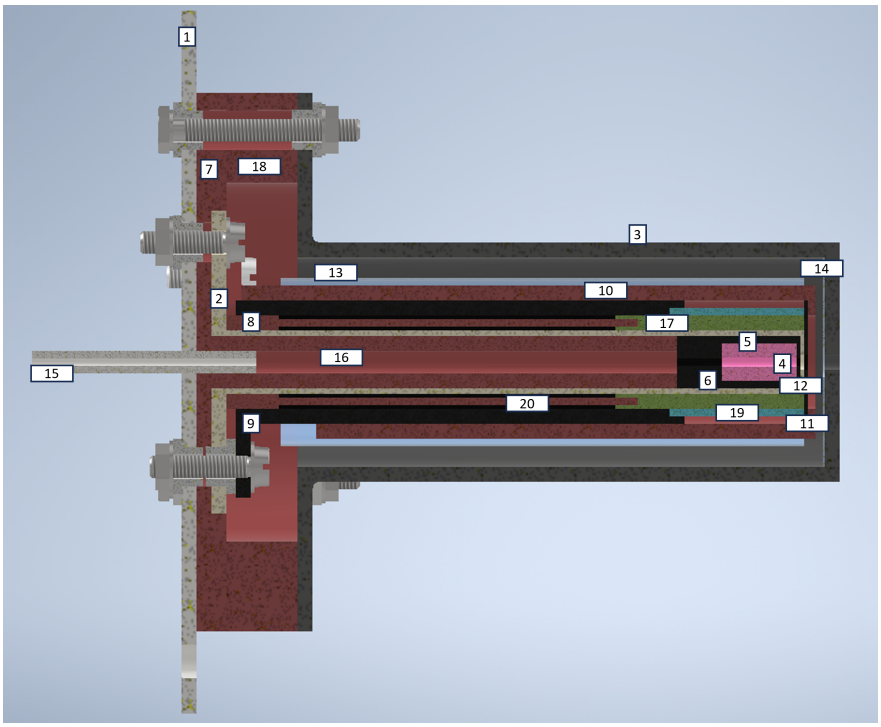

Figure 1. Final HC design cross-sectional view. Labels from 1 to 20 represent the numbering in Table 2.

Table 1. HC critical dimensions.

Dimension	[mm]
Orifice ID	0.5
Orifice Length	1
Insert ID	1.3
Insert OD	5
Insert Length	10
Keeper to orifice distance	2.25
Keeper orifice ID	2
Total cathode Length	88

Table 2. Designation, material, and label number (referring to Fig. 1) of the HC parts.

Part name	Material	Label
Base	Stainless steel	1
Cathode	Molybdenum	2
Keeper	Graphite	3
Insert - LaB_6	LaB_6	4
Graphite layer	Graphite	5
Guide Plate	Graphite	6
Insulator ring	Alumina	7
Heater Sleeve cage 1	Alumina	8
Electric connection heater	Graphite	9
External sleeve	Alumina	10
Disk connect heater	Graphite	11
Orifice	Graphite	12
Thermal shield	Tantalum	13
Shield keeper	Tantalum	14
Feed line	Stainless steel	15
Pusher	Alumina	16
Heater Sleeve cage 2	Boron nitride	17
Spacer ring	Alumina	18
Heater	Tungsten	19
Alumina rods	Alumina	20

B. Thermal simulations

Steady state thermal simulations have been conducted to validate the thermal management of the HC design and minimise its thermal losses. The material properties introduced in the simulation can be found in Table 3, they have been extracted from several providers data sheets. However, since most of the material properties, such as the thermal conductivity, have a dependence on temperature, a tabular input was used to account for this effect when data were available. The table shows mean values. To model the thermal behaviour of the hollow cathode, several assumptions have been considered to simplify the model:

- The base is considered an adiabatic surface.
- All external surfaces, except the base plate, radiate heat to the vacuum chamber at 298.15 K.
- The heater has been modelled as a complete cylinder instead of as a filament in spiral shape to simplify the determination of radiation of the view factors and surfaces seen.
- Convection heat transfer is disregarded in all the model.
- Any fastener (screws, nuts, washers) have been suppressed to simplify the computation of the mesh and the determination view factors.
- Simulations were performed by changing the input heating power iteratively until reaching an approximate temperature of 1575 K in the insert material. This is the temperature taken as the threshold for thermionic emission at ignition. Further details are given in Section II.D.
- Thermal loads due to plasma have not been considered. These thermal simulations are only to evaluate the heater power required for ignition, before the discharge is established. Therefore, it does not include any heat flux coming from the plasma.

Table 3. Material properties used for thermal simulations.

Material	Emissivity	Thermal conductivity [W/(m·K)]	Specific heat [J/(kg·K)]	Melting point [K]
Tantalum	0.3	57.5	140	2996
Stainless Steel	0.7	13.8	480	1670 - 1800
Boron Nitride	0.8	60	960	3246
Molybdenum	0.3	138	251	2896
Graphite	0.85	50	709	3800
Alumina	0.25	32	880	2345
Tungsten	0.42	163.3	132	3695
LaB_6	-	47	-	2528

The simulation results for the final assembled design are showed in Fig. 2. The required heating power to reach the depicted thermal steady state is of 220 W.

A key feature of this final design is its complex heater sleeve with a "bird cage" shape, its assembly is shown in Fig. 5. Its innovative design reduces thermal losses in the axial direction towards the base plate and also avoids short circuits of the cathode tube, with the graphite sleeve and the heater. The temperature drops by 600 K between the downstream end and the upstream end of the bird cage.

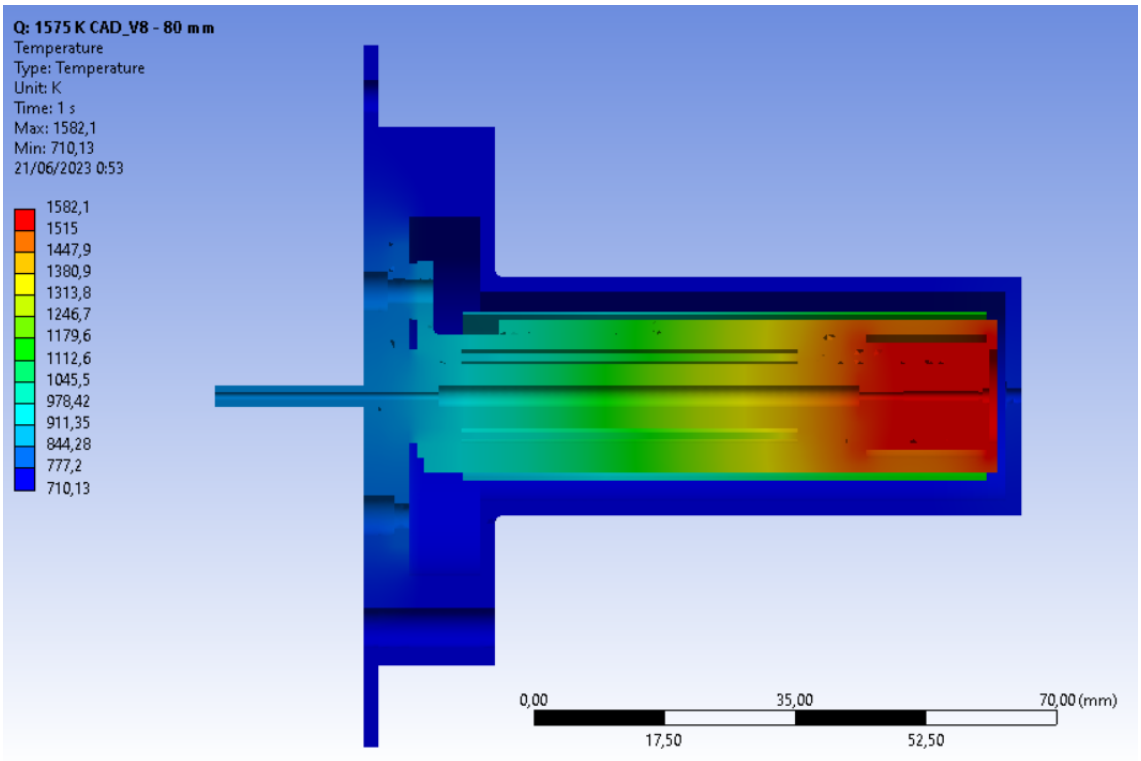

Figure 2. Temperature field results of the final HC design, with a heater power of 220 W. Temperatures around 1575 K (red colour) are reached for the insert region, whereas the bird cage rods introduce a decrease in temperature from 1400-1500 K to 1000-1100 K. The stainless steel base plate is maintained at a temperature below its melting point.

C. Heater design

The sizing of the heater filament and the number of spires has been based on the calculated heating power of 220 W resulting from the thermal simulations presented before. The Tungsten properties used for the computations can be found in Ref. 21. All the input data are gathered in Table 4 and the results obtained are showed in Table 5. The Tungsten resistivity (ρ_W) as function of its temperature, T_h, is estimated as in Ref. 21,

$$\rho_W(T_h) = 48.0 \cdot 10^{-9} \cdot (1 + 4.8297 \cdot 10^{-3} \cdot T_h + 1.663 \cdot 10^{-6} \cdot T_h^2) \tag{1}$$

The number of windings (N_h) was set to 9 to fit the available space and provide sufficient spacing between spires. By fixing a heater filament of wire diameter $t_{h,W} = 0.5$ mm and considering the outer diameter of the BN sleeve ($D_{o,BN}$) the total heater filament length ($L_{h,F}$) is approached as:

$$L_{h,F} = \pi \cdot (D_{o,BN} + t_{h,W}) \cdot N_h. \tag{2}$$

The heater resistance is obtained accounting for its geometry,

$$R_h = \frac{\rho_W \cdot L_{h,F}}{A_h}, \tag{3}$$

then, the current through the heater for a given power (220 W),

$$I_h = \sqrt{\frac{P_h}{R_h}} = 13.36 \text{ A}, \tag{4}$$

and the voltage drop through it would be around 16.47 V.

Table 4. Input data for heater sizing. Resistiviy evaluate at 1575 K.

Inputs	Value
P_h [W]	220
T_h [K]	1585
ρ_W [Ω·m]	6.2×10^{-7}
$t_{h,W}$ [mm]	0.5
$D_{o,BN}$ [mm]	13.4
A_h [m^2]	1.964×10^{-7}

Table 5. Results for heater sizing.

Outputs	Value
$L_{h,F}$ [m]	0.39
N_h [-]	9
I_h [A]	13.36
R_h [Ω]	1.23
V_h [V]	16.47

D. 0D thermionic emission calculations

A simplified analysis of the thermionic emission has been used to determine the minimum emitter temperature for effective emission during ignition. The result of this analysis has been anticipated in the previous section, 1575 K. The model does not account any effect of the plasma generated within the HC. The main assumption here is that for triggering the ionization cascade, a minimum seed current, $I_{seed} = 0.1$ A, is required, which is indeed an arbitrary level, in this case a 10 % of the target HC discharge current. Hereafter, the main equations of this model are presented and the computations are addressed.

The emitted current density can been estimated through the Richardson-Dushman law for thermionic emission (j_{em}), while the Child-Langmuir law equation models the limit set by the space-charge effects (j_{CL}) on the emission:

$$j_{em} = DT_w^2 \cdot \exp\left(\frac{-eW_0}{k_B T_w}\right) \cdot \exp\left(\frac{\sqrt{\frac{e^3 E}{4\pi\epsilon_0}}}{k_B T_w}\right), \tag{5}$$

in which, $E = \dfrac{V_k}{d_{k-o}}$ is a crude estimation of the electric field set by the keeper-to-cathode voltage.

$$j_{CL} = \frac{4\epsilon_0}{9}\sqrt{\frac{2e}{m_e}}\frac{V_k^{3/2}}{d_{k-o}^2} \tag{6}$$

The physical constants are showed in Table 6 and the LaB_6 material properties used are given in Table 7. The Richardson coefficient (D) and the work function (W_0) for LaB_6 have been retrieved from Ref. 22. Defining the emitter internal area $A_e = 40.841$ mm^2 and a minimum keeper-orifice distance $d_{k-o} = 2.25$ mm, the only free parameters are the emitter wall temperature, T_w, and the keeper voltage, V_k. A parametric study with these two variables has been carried out to determine an optimum range of temperatures and keeper

voltages for ignition. The results in Fig. 3 show that the seed current of 0.1 A can be met by an insert temperature around 1575 K and a keeper voltage over 300 V. This keeper voltage is rather large but still falls within the range typically used for low-current HCs[5;14]. This is a benchmark value for future coupling tests with 100 - 400 W CHTs.

Table 6. Constant parameters.

Constant	Value
ϵ_0 [F/m]	8.85 E-12
σ [W/(m^2 K^4)]	6.67 E-8
e [C]	1.6 E-19
k_b [J/K]	1.38 E-23
m_e [kg]	9.1 E-31

Table 7. Parameters for thermionic emission.

Variable	Value
A [mm^2]	40.84
d_{k-o} [mm]	2.25
D [A/(m^{2}K^2)]	29×10^4
W_0 [eV]	2.66

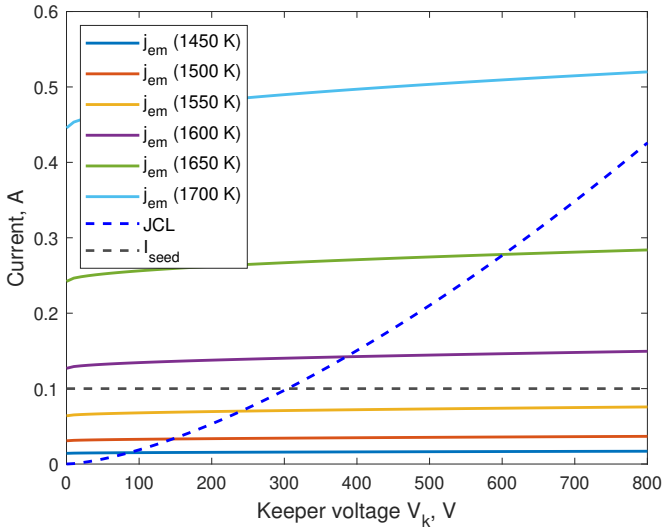

Figure 3. Thermionic emission results for d_{k-o} = 2.25 mm at different temperatures (solid lines). The Child law curve (dashed blue line) represents the limit for the extracted current and the solution cannot be above this line. For an insert wall temperature T_w = 1575 K a keeper voltage of at least V_k = 300 V is required to produce a current I_{seed} = 0.1 A.

III. Final Hollow Cathode design

After completing the design process, the assembled HC prototype is showed in Fig. 4, with internal details of the heater sleeves and heater assembly in Fig. 5. It is important to highlight that this low-current HC device is completely dismountable and it allows for the replacement of any damaged part. This is a key feature for laboratory testing since it makes it possible to push the cathode operating conditions over standard regimes. The device does not feature any welded parts, which allows for avoided complicated techniques suited for refractory metals.

The heater, one of the critical components due to the thermal loads it has to withstand, has been manufactured by wrapping a tungsten filament of 0.5 mm diameter around the boron nitride cathode sleeve, as shown in Fig. 5. A slot (see Fig. 5b) was machined in the graphite sleeve (9 in Fig. 1) to improve the electrical connection between the heater filament end and part 9 which serves as one of the heater electrical terminals. The other end of the heater is in contact with the molybdenum cathode tube (2 in Fig. 1) which serves as the other electrical terminal. The contact is ensured by pressing the filament between the cathode tube tip, two Tantalum foil washers and a graphite disk (11 in Fig. 1) within the alumina tube (10 in Fig. 1).

Figure 4. UC3M low current HC assembled prototype.

(a) Bird cage heater sleeve assembly (b) Heater filament assembly

Figure 5. Heater sleeves and filament assembly. (a) The bird-cage sleeve is composed of two cylinders in boron nitride (top) and alumina (bottom) joined by 6 alumina rods to avoid electrical contact between the cathode tube and the graphite sleeve. (b) The graphite sleeve has an indentation to ensure electrical connection between the heater and graphite.

IV. Experimental setup

The experiments were performed in the vacuum chamber of the UC3M [23]. It consists of a non-magnetic stainless-steel cylindrical vessel which is 3.5 m long and 1.5 m in diameter. The chamber has a dry mechanical pump (Leyvac LV80), and two magnetically levitated turbomolecular pumps (Leybold MAGW2.200iP). Moreover, the chamber is equipped with three cryo-panels (Leyvac 140 T-V). Its performance gives a total pumping speed of 37000 l/s of Xe, reaching an ultimate pressure of 10^{-7} mbar in dry conditions. The vacuum chamber achieves a base pressure between $2{\times}10^{-6}$ and $8.4{\times}10^{-6}$ mbar for a Xenon flow from 1 to 8 sccm.

The electric scheme of the cathode experiment in diode mode using a sacrificial anode is depicted in Fig. 6. It is composed of three direct-current (DC) power supplies (Keeper, Anode, Heater) that share a reference point or cathode terminal. A Bronkhorst EL-FLOW Select mass flow controller provides the required mass flow rate of Xenon from a pressurised tank. Experiments were conducted with and without grounding the cathode terminal. The anode is a stainless steel disk of 10 cm in diameter and 1.5 cm of thickness.

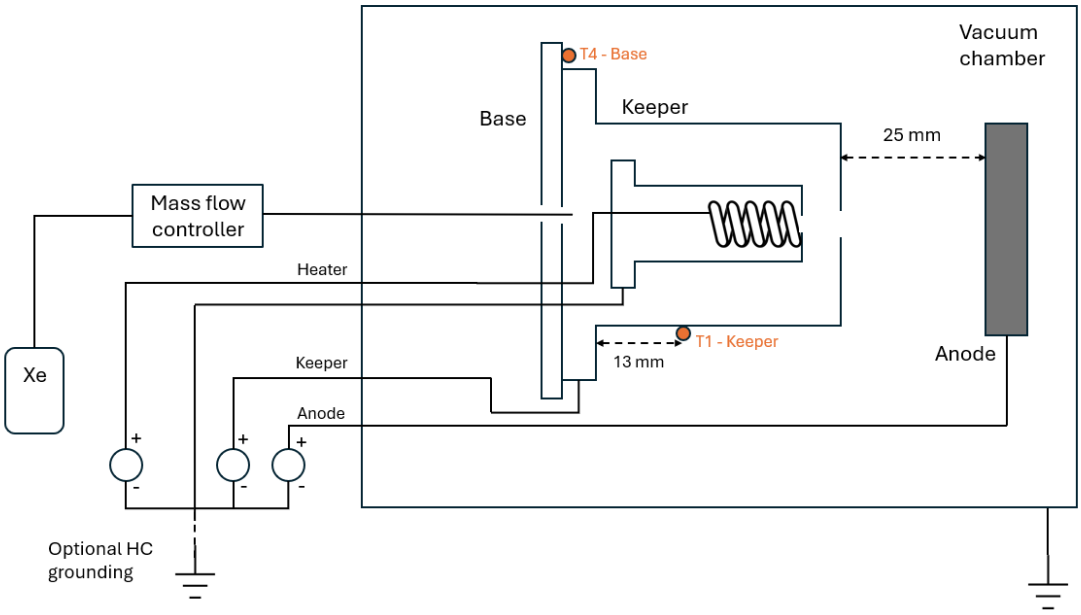

Figure 6. Experimental setup used for HC testing. There are three DC power supplies connected to the heater, keeper and anode. The heater line returns through the cathode tube base. The HC grounding is optional.

V. Experimental results

A. Ignition procedure

Prior to the first ignition, a cathode conditioning was performed by slowly ramping the heater current up and then down, while feeding Krypton to the injector. This is not only to characterize the heater behaviour but also to let the components of the assembly outgas and expand thermally for the first time.

The ignition procedure is the usual one for HCs. In this case heater current (I_h) is increased at a rate of 2 A/min, while the Xe mass flow rate, ($\dot{m}$) was set to 2 sccm. When I_h reached 12 A (180 W of heating power), the current was increased at a slower rate to properly characterize the ignition conditions. The thermal simulations showed that a heating power around 220 W is required to ignite. From this point onwards, the keeper electrode was biased and the voltage was ramped up from 100 to 800 V, while the mass flow rate was increased to 10 sccm. If ignition was not achieved, the heating power was increased by 0.5 A and the same range of V_k was tested. Ultimately, if ignition was not reached at $I_h = 14$ A, the mass flow rate was increased up to 15 sccm, in steps of 1 sccm.

Ignition was first attempted unsuccessfully with Krypton, then more than five ignitions were performed successfully with Xe. The heater voltage and power as a function of the heater current is depicted in Fig. 7 for the conditioning and the last heating ramp. The variation in heating power between the initial conditioning and the last heating remained below 5 %. Small differences in the heater resistivity between cycles may be caused by change of shape of the tungsten filament after each heating and cooling cycle which can create short circuits, contacts, changes in tungsten structure, or oscillations in V_h values due to transients.

Table 8 shows that the HC ignites within 10 - 15 sccm, consuming 267 - 305 W of heating power, and keeper voltages in the range 550 - 850 V. Whenever one of the parameters was close to the lower bound, the other ones had to be increased to compensate for it. Two thermocouples were installed on the HC, see Fig. 6, to monitor its thermal behaviour. The temperatures measured by the thermocouples showed that steady state was never reached during ignition. One of the consequences is the lack of agreement between the thermal simulations (in steady state) and the measured temperature during the experiment (long transient). Therefore, it could be possible to ignite the HC at a lower heating power or mass flow rate if enough time was given to reach steady state and therefore potentially a higher emitter temperature. To sum up, the ignition is successful and repeatable in the ranges presented in Table 8.

Table 8. Ignition conditions.

Experiment	Xe Mass flow [sccm]	I_h [A]	V_h [V]	P_h [W]	V_k [V]	V_a [V]
1	14	14.66	20.8	304.9	576	50
2	10	14.00	19.1	267.4	850	500
3	12	14.50	20.0	290.0	570	300
4	15	14.50	19.6	284.2	675	600
5	12	14.50	19.8	287.1	600	100

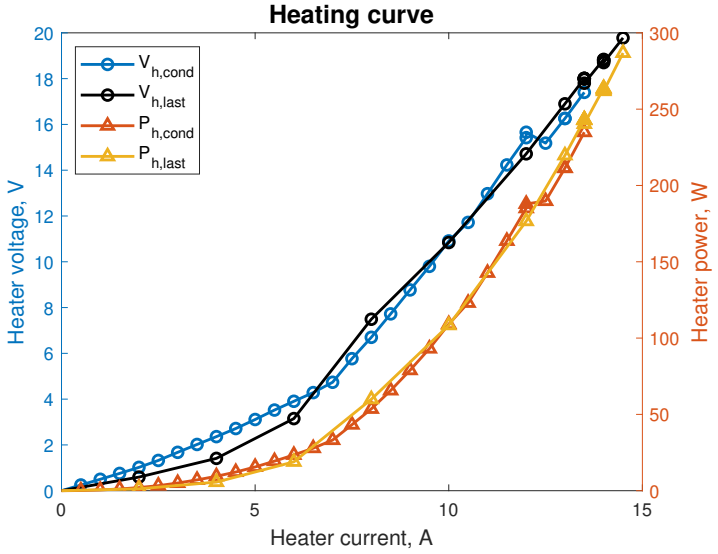

Figure 7. Heating curve comparison for initial conditioning and the last Xe ignition. The subscript "conditioning" represents the former whereas "last" refers to the latter.

B. Diode mode characterization

The objective of the diode mode testing campaign against a sacrificial anode is to characterize the operating range of the HC, and to demonstrate its capability of operating in the sub-amp regime at low $\dot{m}$. After the ignition process, $\dot{m}$ was decreased to 1 sccm for an anode current $I_a = 1$ A while powering off the heater and the keeper. Therefore, the HC was self-heated and with the keeper floating. Once this point was reached, I_a and $\dot{m}$ were changed in the ranges 0.6 - 2.5 A and 0.6 - 1.5 sccm, respectively. Tests were performed for grounded and ungrounded HC configurations.

Regarding the anode voltage in Fig. 8a, a non-monotonic behaviour can be observed with a minimum between 1 and 1.5 A of anode current for the grounded configuration. For discharge currents below 1.5 A, V_a increases as I_a is reduced. Overall, at constant discharge current, the anode voltage always increases when $\dot{m}$ decreases, therefore it takes more electrical power to extract the electrons when a low amount of gas is available (Fig. 10). However, beyond the minimum of $V_a - I_a$, the positive slope of the curve becomes smaller as the mass flow rate is increased. Meaning that at constant $\dot{m}$, extracting additional current (past the minimum of Va - Ia) still requires more power, in this situation, the amount of power required per extra ampere is smaller at high flow rates. Similar behaviours can be found in the literature for HC operating in self-heated mode with an anode[24;25;26]. Fig. 8b shows the anode-to-cathode voltage for the ungrounded case, overall, lower voltages are obtained for the same pair of $\dot{m}$ and I_a.

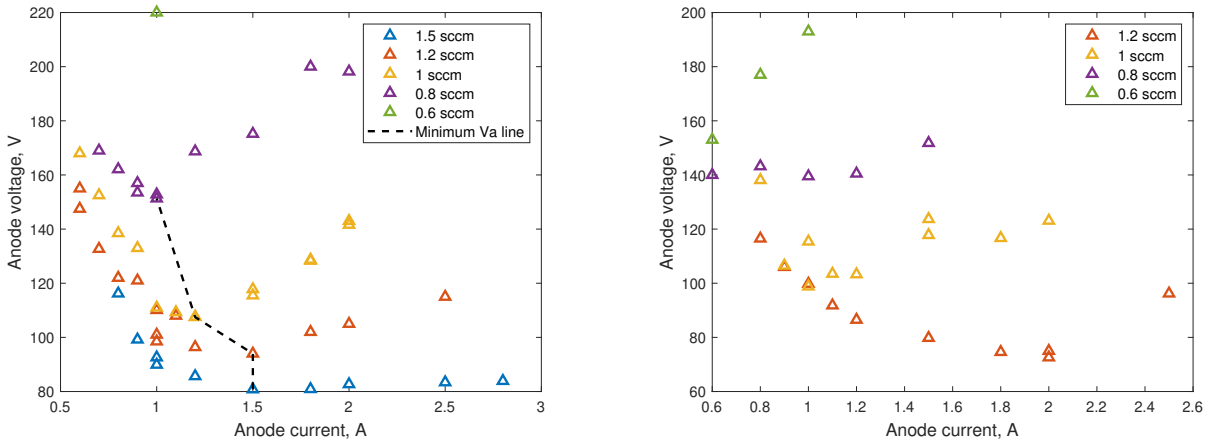

(a) Grounded anode voltage evolution

(b) Ungrounded anode voltage evolution

Figure 8. Anode voltage against anode current at different Xe mass flow rates. (a) with the cathode grounded and (b) with the cathode ungrounded.

Figure 9 shows that the keeper voltage increases monotonically with the anode current, regardless of $\dot{m}$. In all figures keeper and anode voltages are referred to cathode voltage (0 for ground or cathode reference potential for ungrounded). At 1 sccm there is no big difference between the floating and grounded configurations, while at 0.8 sccm, the ungrounded configuration yields to slightly lower values for the keeper and anode voltages (compared in detail in 9b). In a similar way as for Vk, at 1 sccm the voltage anode response is not affected by the cathode grounding or ungrounding, while at 0.8 sccm, again, lower anode voltage is measured for the ungrounded case. This means that presumably the self-heating mechanism is influenced by the (un)grounded state. A slightly larger anode power (4-30 W) is required to extract the same current for a given mass flow rate. Further tests are required to explore this difference in the results.

The little data available below 0.8 sccm is the result of the difficulties to keep the HC in self-sustained mode. Some solutions might rely on adding some heating or keeper power as done by Domonkos[4], Kokal[27], or Potrivitu[17].

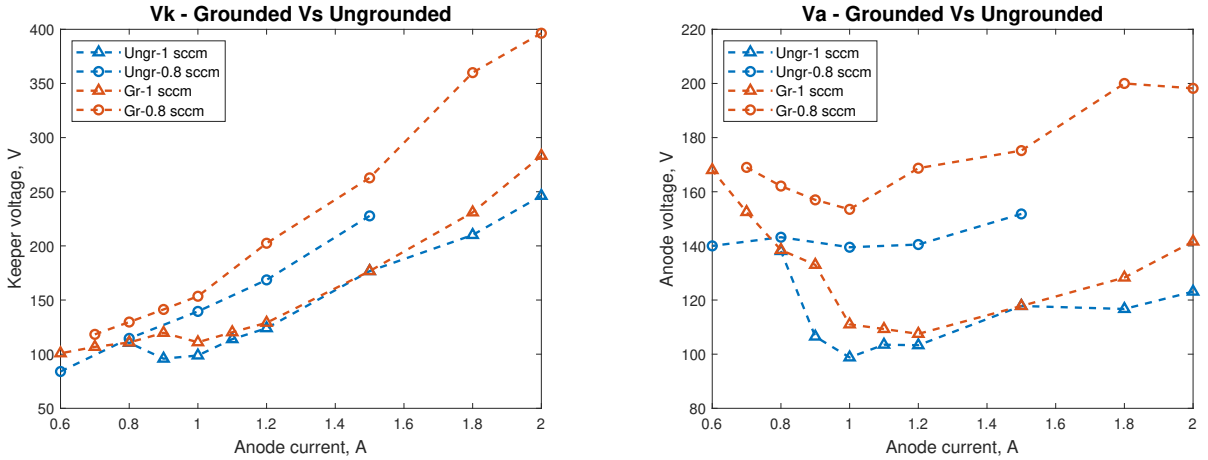

(a) Keeper voltage

(b) Anode voltage

Figure 9. Comparison of the evolution of V_k (a) and Va (b) against I_a, for two mass flow rates, between the grounded (red) and ungrounded (blue) HC.

To roughly assess if the power consumed by the HC is reasonable in self-sustained operation in the hypothetical coupling to the CHT, the anode power is depicted in Fig. 10. This shows an increase in power as I_a rises. At any current, the larger the mass flow rate the lower the power required to sustain the discharge.

This is because a higher mass flow rate will lead to higher neutral and plasma densities, thus making electron extraction easier and enhancing emitter heating due to plasma bombardment. According to these results, it is plausible to conclude that this cathode could be used as a neutralizer for the CHT [7].

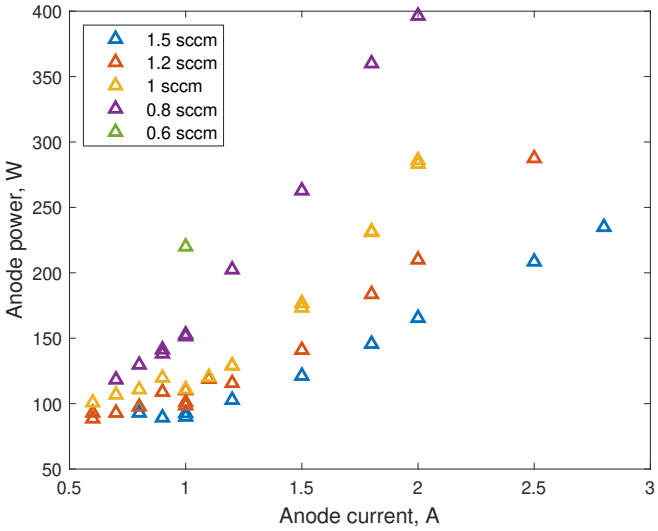

Figure 10. Evolution of the anode power with the current for different Xe mass flow rates for the grounded configuration.

VI. Conclusions

This paper has presented the design, assembly and first validation test of a low-current hollow cathode. The cathode has a modular design which makes it fully dismountable to allow the replacement and modification of components. The main configuration and materials selection was conducted based on a trade-off among the research of the state-of-art on HCs. Furthermore, the HC geometry features a LaB_6 insert heated with a tungsten coil, and an orifice, all enclosed within a graphite keeper. The sizing of the cathode has been supported by the combination of a 0D model of the thermionic emission, the thermal/electrical characterisation of the heater filament, and thermal simulations of the complete HC model, in order to minimize heat losses and select the most appropriate geometry.

The first part of the experimental campaign characterised the heater I-V curves. The following tests consisted in the standalone operation of the HC in diode mode against an anode plate. Ignitions conditions were carefully analysed, identifying some thresholds for a Xenon flow rate of 10 sccm, a keeper voltage over 570 V and a heating power over 260 W. Once the HC is ignited, self-sustained operation is established without heater and keeper power. The device was tested at several mass flow rates, sweeping the anode discharge current from 0.6 to 2.8 A. The data retrieved shows that the device is very stable in the range 0.8 to 1.5 sccm of Xe. The trends obtained have been compared with the results of similar self-sustained, low-current HC operating in diode mode with an anode. Analysis of the required power for electron extraction gave a power from 88 to 130 W for the desired range dictated by the future coupling with the CHT. As a result, the performance of the HC in the ranges set by the requirements has been validated, except for the required power which is slightly larger than 100 W for most test points.

Future work involves the modification of the downstream end of the cathode by adding a ceramic disk to avoid Xe back-flow during ignition, thus relaxing ignition conditions. Moreover, more tests will be carried out focusing on the low mass flow rate limit, below 0.8 sccm, to determine if additional heat or keeper current can allow for maintaining help to keep the discharge. Finally, the HC will be coupled to the low-power CHT developed by UC3M.

Acknowledgments

This work has been supported by the project COMIT funded by the Spanish Government (grant PDC2021-120911-I00).

References

[1] Dan Lev, Roger M. Myers, Kristina M. Lemmer, Jonathan Kolbeck, Hiroyuki Koizumi, and Kurt Polzin. The technological and commercial expansion of electric propulsion. *Acta Astronautica*, 159:213–227, 2019.

[2] D Pedrini, F Cannelli, R Hadavandi, C Ducci, U Cesari, T Misuri, M Andrenucci, F Paganucci, et al. Recent advances in low-current hollow cathodes at sitael. In *Proceedings of the 36th International Electric Propulsion Conference*, 2019.

[3] Dan M Goebel, Ron M Watkins, and Kristina K Jameson. Lab6 hollow cathodes for ion and hall thrusters. *Journal of Propulsion and Power*, 23(3):552–558, 2007.

[4] Matthew T Domonkos, Michael J Patterson, and Alec D Gallimore. Low-current, xenon orificed hollow cathode performance for in-space applications. *Journal of propulsion and power*, 19(3):438–443, 2003.

[5] George-Cristian Potrivitu, Yufei Sun, Muhammad Wisnuh Aggriawan bin Rohaizat, Oleksii Cherkun, Luxiang Xu, Shiyong Huang, and Shuyan Xu. A review of low-power electric propulsion research at the space propulsion centre singapore. *Aerospace*, 7(6):67, 2020.

[6] Adrian Heiler, Katja Wätzig, Martin Tajmar, Roland Friedl, Riccardo Nocentini, and Ursel Fantz. Work function performance of a c12a7 electride surface exposed to low pressure low temperature hydrogen plasmas. *Journal of Vacuum Science Technology A*, 39:013002, 01 2021.

[7] T. Perrotin, A. E. Vinci, S. Mazouffre, J. Navarro-Cavallé, P. Fajardo, and E. Ahedo. Measurements of xenon ions and atoms velocity in cylindrical hall thruster with laser-induced fluorescence spectroscopy. In *10th EUCASS Conference*, Lausanne, Switzerland, July 9–13, 2023.

[8] Tatiana Perrotin, Alfio E Vinci, Stéphane Mazouffre, Pablo Fajardo, Eduardo Ahedo, and Jaume Navarro-Cavallé. Far-field plume characterization of a low-power cylindrical hall thruster. *Journal of Applied Physics*, 136(4), 2024.

[9] George-Cristian Potrivitu, Luixiang Xu, Igor Levchenko, Shiyong Huang, Yufei Sun, Muhammad Wisnuh Aggriawan Rohaizat, Lim Jian Wei Mark, Kateryna Bazaka, and Shuyan Xu. Mode transition in a low-current lab6 hollow cathode for electric propulsion systems for small satellites. 09 2019.

[10] Michael S. McDonald, Natalie R.S. Caruso, and Margaret M. Mooney. Multiple orifices and integrated radiation shielding in the hollow cathode keeper. *IEPC-2019-929*.

[11] Dan Lev, Ioannis Mikellides, Daniela Pedrini, Dan Goebel, Benjamin Jorns, and Michael Mcdonald. Recent progress in research and development of hollow cathodes for electric propulsion. *Plasma Physics*, 3, 06 2019.

[12] Master thesis University of Alabama in Huntsville Ryan P. Gott. The development and analysis of a heaterless, insertless, microplasma-based hollow cathode. 2017.

[13] Dan M. Goebel, Ron M. Watkins, and Kristina K. Jameson. Lab6 hollow cathodes for ion and hall thrusters. *Journal of Propulsion and Power*, 23(3):552–558, 2007.

[14] Daniela Pedrini, Federico Cannelli, Ruzbeh Hadavandi, Cosimo Ducci, Ugo Cesari, Tommaso Misuri, Mariano Andrenucci, and F. Paganucci. Recent advances in low-current hollow cathodes at sitael. 09 2019.

[15] G.A. Parakhin, R.S. Pobbubniy, A.N. Nesterenko, and A.P. Sinitsin. Low-current cathode with a bao based thermoemitter. *Procedia Engineering*, 185:80–84, 2017. Electric Propulsions and Their Application.

[16] Antonio Gurciullo, Vasiliki Papaefthimiou, Paul Lascombes, Stéphane Mazouffre, Fabian Plaza, and Angel Post. Examination of C12A7 electride work function and surface composition by means of XPS, UPS and thermionic emission measurements. In *37th International Electric Propulsion Conference*, Electric Rocket Propulsion Society - IEPC 2022 Proceedings, Cambridge, United States, June 2022.

[17] G.-C. Potrivitu, L. Xu, S. Huang, M. W. A. B. Rohaizat, and S. Xu. Discharge mode transition in a Krypton-fed 1 A-class LaB6 cathode for low-power Hall thrusters for small satellites. *Journal of Applied Physics*, 127(6):064501, 02 2020.

[18] Alex Nikrant. Development and modelling of a low current lab6 heaterless hollow cathode. *Master thesis Virginia Polytechnic Institute*, 2019.

[19] Alexander Daykin-Iliopoulos, Igor Golosnoy, and Steve Gabriel. Thermal profile of a lanthanum hexaboride heaterless hollow cathode. 10 2017.

[20] A. Montero. Low-current hollow cathode design- master thesis uc3m, 2023.

[21] David R. Lide. *CRC Handbook of Chemistry and Physics*. CRC Press, 1995.

[22] Dan Goebel and Ira Katz. *Fundamentals of Electric Propulsion: Ion and Hall Thrusters*. 2008.

[23] M. R. Inchingolo, M. Merino, M. Wijnen, and J. Navarro-Cavallé. Thrust measurements of a waveguide electron cyclotron resonance thruster. *Journal of Applied Physics*, 135(9):093304, 03 2024.

[24] Romain Joussot, Lou Grimaud, and S. Mazouffre. Examination of a 5 a-class cathode with a lab 6 flat disk emitter in the 2 a-20 a current range. *Vacuum*, 146, 09 2017.

[25] Fan Li, Tianhang Meng, Zhongxi Ning, Chenying Li, Ao Han, Yingting Li, and Daren Yu. Improved performance of low current hollow cathode by inserted emitter core. *Vacuum*, 207:111492, January 2023.

[26] V. Vekselman, Ya. E. Krasik, S. Gleizer, V. Tz. Gurovich, A. Warshavsky, and L. Rabinovich. Characterization of a heaterless hollow cathode. *Journal of Propulsion and Power*, 29(2):475–486, 2013.

[27] Huseyin Kurt, Ugur Kokal, Nazli Turan, and Murat Celik. Note: Coaxial-heater hollow cathode. *Review of Scientific Instruments*, 88:066103, 06 2017.